www.lajss.org
Latin American Journal of Solids and Structures 2 (2005) 269–290

Sudden contraction in a turbulent flow with a porous insert

R.M. Orselli and M.J.S. De Lemos*

Laboratório de Computação em Fenômenos de Transporte – LCFT
Departamento de Energia – IEME, Instituto Tecnológico de Aeronáutica – ITA
12228 – 900 – São José dos Campos, SP – Brazil

Abstract

The purpose of this work is to investigate the influence of a porous insert in an incompressible turbulent flow in a pipe that suffers a sudden contraction. The Reynolds number considered is 158,000 based on the pipe outlet diameter. The flow equations are discretized by using the control volume method and the SIMPLE algorithm is applied for the velocity-pressure coupling. In all cases, the macroscopic $k-\varepsilon$ Low-Reynolds turbulence model is employed. For an initial numerical validation a simulation is carried out without the porous insert in order to be compared with an experimental result. Subsequently, a porous insert is considered in the numerical simulations. The flow losses obtained with the porous insert are calculated and compared with those obtained from the calculations without the porous insert.

Keywords: Turbulent flow, porous media, numerical simulation, sudden contraction.

1 Introduction

There are several applications in industry and science which involve flows through permeable media, such as, engineering systems in oil extraction, filters, flow through forests, crops and cooling in electronic equipment. Further, when a flow passes through a sudden contraction, the flow direction changes abruptly and a recirculating bubble is observed past the contraction. This phenomenon is known in the literature as *vena contracta*.

Analysis of flows in pipes with sudden contraction has been subject of numerous publications since the middle of the 19th century. In the work of [38], experimental values of the minimum jet contraction area, S_c, as a function of σ, where σ is the ratio between the pipe outlet cross section area (S_{ex}) and its inlet section area (S_{in}), were presented. In [34], experimental values of minor losses were shown as a function of σ for turbulent flows. Also in [18], experimental data of minor losses for laminar and turbulent flows for a wide range of contraction ratios were presented. Measurements of pressure drop for low Reynolds numbers and a discussion about

*Corresp. author Email: delemos@ita.br Received 26 September 2005; In revised form 13 October 2005

Notation

σ	Contraction area ratio, dimensionless
S_{in}, S_{ex}	Respectively, the inlet and outlet pipe cross section area
S_c	Minimum jet contraction area
k	Turbulent kinetic energy per mass unity
ε	Dissipation rate of k
x	Axial coordinate
r	Radial coordinate
U_{in}, U_{ex}	Respectively, the inlet and outlet pipe streamwise bulk velocity
d_{in}, d_{ex}	Respectively, the inlet and outlet pipe diameter.
r_{in}, r_{ex}	Respectively, the inlet and outlet pipe radius
l_{in}, l_{ex}	Pipe length, respectively, upstream and downstream the pipe contraction
a	Porous insert thickness
$\bar{\mathbf{u}}_D$	Time average Darcy or superficial velocity vector
$\bar{\mathbf{u}}$	Time average velocity vector
ϕ	Porosity
c_F	Forchheimer coefficient
p	Thermodynamic pressure
ρ	Density
μ	Dynamic viscosity
K	Porous medium permeability
μ_{t_ϕ}	Macroscopic turbulent viscosity
c_μ, σ_k, σ_ε, c_1, c_2, c_k	Non-dimensional constants of the turbulence model
f_2, f_μ	Damping function used in the $k-\varepsilon$ Low Reynolds Model
n	Coordinate normal to the wall
n_p	Distance of the first volume from the wall
μ_t	Turbulent viscosity
n_p^+	Non-dimensional distance of the first volume from the wall
n^+	Non-dimensional distance from the wall
u_τ	Friction velocity
ν	Kinematic viscosity
τ_w	Shear stress on the wall
Re_{in}, Re_{ex}	Reynolds number, respectively, based on the inlet and outlet pipe diameter
h_c	Minor losses due to the contraction
k_c	Contraction minor loss coefficient
Cp	Pressure coefficient
p_{ref}	Reference pressure
KN	Normalized turbulent kinetic energy, values between 0 and 1
C_f	Friction coefficient

the pressure drop problem due to a sudden contraction for laminar flows was reported in [11]. Numerical results for streamlines, velocity profiles and pressure losses were presented in [36], which have considered three different contraction ratios for a Reynolds numbers based on the pipe inlet diameter ranging from 0 to 200. Experimental and numerical results of velocity profiles for some cross sections upstream and downstream the contraction and the dimensions of the recirculating bubble past the contraction were reported in [15]. In their work, it was investigated laminar flows for $\sigma = 0.285$.

Concerning modeling of macroscopic transport equations in porous media, if time fluctuations and spatial deviations of the flow are considered, there are two possible methodologies to follow: *a*) application of volume-averaging operator followed by time-averaging [2, 16, 23, 37], or *b*) use of time-averaging before volume-averaging is applied [20, 21, 24, 25, 35]. In fact, these two sets of macroscopic transport equations are equivalent when examined under the recently established double decomposition concept [13, 28, 29, 33]. The double-decomposition of flow led to a better characterization of the flow turbulent kinetic and was a step before detailed numerical solutions of the flow equations were carried out [31]. Calculations were needed for adjusting the model considering both the High-Reynolds $k-\varepsilon$ closure [32] and the low-Reynolds version of it [31].

Many articles have recently been published in the literature considering numerical simulations for turbulent flows past a sudden expansion, [4, 6, 8, 10], or contraction, [3, 5, 7, 9], of a planar channel partially filled with a porous insert using both linear and non-linear turbulence models. Therein, parameters such as porosity, permeability, thickness of the porous insert were varied in order to analyze their effects on the flow pattern. Also, the work of [26] has studied a steady turbulent flow in a pipe with sudden contraction where a porous insert was placed downstream the contraction. Other recent works concerning numerical simulations of turbulent flows in channels with porous insertions should be mentioned. As such, the work of [12] has studied a turbulent flow over a 2D backward facing step where a porous insert has been placed immediately downstream of the step in order to investigate the influence of the porous insert thickness, permeability and Forchheimer's constant on the flow behavior. Also, the work of [14] has analyzed the effect of porosity, permeability and Reynolds number on the flow pressure drop in a parallel-plate channel containing porous fins.

Based on the foregoing, the objective of this article is to analyze the porous insert influence on a turbulent flow in a pipe which suffers a sudden contraction. The numerical tool to be used is the control volume technique in a generalized coordinate system. The turbulent model employed is the macroscopic $k-\varepsilon$ Low-Reynolds turbulence model. Firstly, the numerical result for a clear sudden contraction is compared with the experimental results available in the literature. Afterwards, the same pipe is investigated with a porous insert placed downstream the contraction. The new flow behavior is analyzed by comparing the two cases, namely, with and without the porous insert. Attention is given to the pipe minor losses and also to the flow patterns at the pipe contraction region.

2 Geometry and grid under consideration

Figure 1a shows the minimum jet contraction area, S_c, where the effective flow area is reduced due to the recirculation on the pipe walls downstream the contraction. This area reduction (*vena contracta*) increases even more the minor losses, mainly during the expansion past S_c section. Figure 1b presents a sketch of the porous insert in the pipe. In Figs. 1a and 1b, U_{in} and U_{ex} are the streamwise bulk velocities, l_{in} and l_{ex} are the pipe lengths, d_{in} and d_{ex} or $2r_{in}$ and $2r_{ex}$ are the pipe diameters and a is the porous insert thickness. In Figs. 1a and 1b, the subscripts in and ex represent the pipe inlet and outlet, respectively.

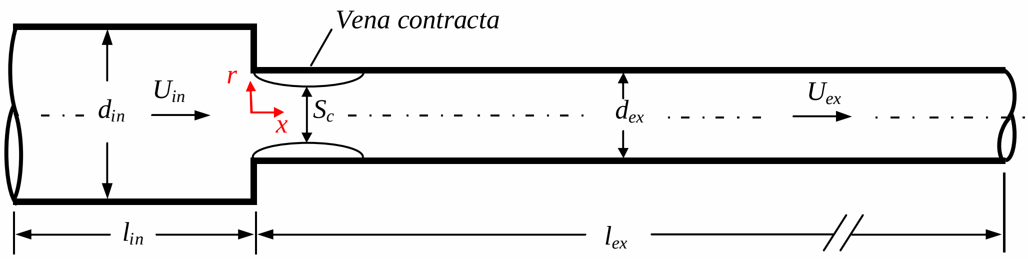

(a)

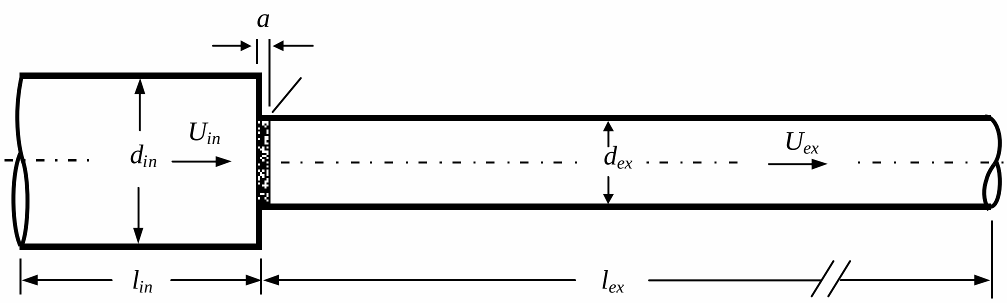

(b)

Figure 1: Simple sketch of the pipe geometry. a) *vena contracta*, b) Porous insert

Figure 2 shows a partial view of the computational domain at the pipe contraction region, where a two-dimensional axisymmetric mesh is presented, having 139 x 141 and 259 x 56 control volumes, respectively, upstream and downstream the pipe contraction. There is a high concentration of grid points close to the wall and towards to the pipe contraction corner. In order to minimize numerical oscillations, the grid points are also concentrated at the interface between the porous insert and the clear medium (Fig. 2).

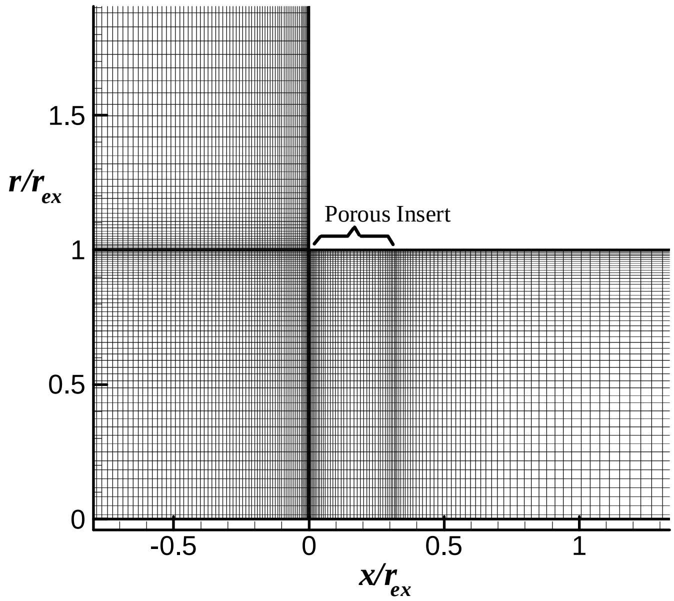

Figure 2: Partial view of the computational grid at the pipe contraction region.

3 Governing equations

Governing equations used in this work are fully documented in [29–31] and for that reason their derivation need not to be repeated here. Basically, a macroscopic form of the time-averaged equations is obtained by taking the volumetric average of the entire equation set. In this development, the porous medium is considered to be rigid, homogeneous and saturated by an incompressible fluid. Also, all physical properties are kept fixed.

The equations that govern turbulent flow in porous medium (neglecting the transient and gravitational terms) are given as follow:

The macroscopic continuity equation is given by,

$$\nabla \cdot \bar{\mathbf{u}}_D = 0 \tag{1}$$

where $\bar{\mathbf{u}}_D$ is the seepage velocity or Darcy velocity. In Eq.(1) the Dupuit-Forchheimer relationship, $\bar{\mathbf{u}}_D = \phi \langle \bar{\mathbf{u}} \rangle^i$, has been used, where ϕ is the porous medium porosity and $\langle \bar{\mathbf{u}} \rangle^i$ identifies the intrinsic (liquid) average of the local velocity vector $\bar{\mathbf{u}}$ [17].

The macroscopic momentum equation can be written as,

$$\rho\nabla\cdot(\frac{\bar{\mathbf{u}}_D\,\bar{\mathbf{u}}_D}{\phi}) = -\nabla(\phi\langle\bar{p}\rangle^i) + \mu\nabla^2\bar{\mathbf{u}}_D + \nabla\cdot(-\rho\phi\langle\overline{\mathbf{u}'\mathbf{u}'}\rangle^i) - \left[\frac{\mu\phi}{K}\bar{\mathbf{u}}_D + \frac{c_F\phi\rho|\bar{\mathbf{u}}_D|\bar{\mathbf{u}}_D}{\sqrt{K}}\right] \tag{2}$$

where the correlation $-\rho\overline{\mathbf{u}'\mathbf{u}'}$ appears after application of the time-average operator to the local instantaneous momentum equation. Further, applying the volume-average procedure to the entire momentum equation (see [29] for details), results in the term $-\rho\phi\langle\overline{\mathbf{u}'\mathbf{u}'}\rangle^i$ of Eq.(2). This term is called here the Macroscopic Reynolds Stress Tensor (MRST). Then, making use again of the $\bar{\mathbf{u}}_D = \phi\,\langle\bar{\mathbf{u}}\rangle^i$ results, finally, in Eq.(2). In addition, the last two terms in the right hand side of Eq.(2) represent the Darcy-Forchheimer contribution where the constant c_F is the Forchheimer coefficient. Also, $\langle\bar{p}\rangle^i$ is the intrinsic average pressure of the fluid, ρ is the fluid density, μ represents the dynamic fluid viscosity and K is the porous medium permeability.

The term MRST, in Eq.(2), is modeled considering the Boussinesq concept for clear fluid as follows,

$$-\rho\phi\langle\overline{\mathbf{u}'\mathbf{u}'}\rangle^i = \mu_{t_\phi}2\langle\bar{\mathbf{D}}\rangle^{\mathbf{v}} - \frac{2}{3}\phi\rho\langle k\rangle^i\mathbf{I} \tag{3}$$

where, $\mathbf{I}$ is the unity tensor, $\langle k\rangle^i$ is the intrinsic average of the turbulent kinetic energy, μ_{t_ϕ} is the macroscopic turbulent viscosity and,

$$\langle\bar{\mathbf{D}}\rangle^v = \frac{1}{2}\left[\nabla(\phi\langle\bar{\mathbf{u}}\rangle^i) + [\nabla(\phi\langle\bar{\mathbf{u}}\rangle^i)]^T\right] \tag{4}$$

is the macroscopic deformation tensor. The macroscopic turbulent viscosity, μ_{t_ϕ} , used in Eq.(3) is modeled similarly to the case of clear fluid and a proposal for it was presented in [29] as,

$$\mu_{t_\phi} = \rho c_\mu f_\mu \frac{\langle k\rangle^{i^2}}{\langle\varepsilon\rangle^i} \tag{5}$$

where $\langle\varepsilon\rangle^i$ is the intrinsic average of the dissipation rate of k.

The macroscopic transport equations for $\langle k\rangle^i = \langle\overline{\mathbf{u}'\cdot\mathbf{u}'}\rangle^i/2$ and $\langle\varepsilon\rangle^i = \mu\langle\overline{\nabla\mathbf{u}' : (\nabla\mathbf{u}')^T}\rangle^i\Big/\rho$ in the $k-\varepsilon$ High-Reynolds form were proposed in [29] and, also, adjusted for the $k-\varepsilon$ Low-Reynolds [31] as follows,

$$\rho\nabla\cdot(\bar{\mathbf{u}}_D\langle k\rangle^i) = \nabla\cdot\left[(\mu + \frac{\mu_{t_\phi}}{\sigma_k})\nabla(\phi\langle k\rangle^i)\right] + P^i + G^i - \rho\phi\langle\varepsilon\rangle^i \tag{6}$$

$$\rho\left[\nabla\cdot(\bar{\mathbf{u}}_D\langle\varepsilon\rangle^i)\right] = \nabla\cdot\left[(\mu + \frac{\mu_{t_\phi}}{\sigma_\varepsilon})\nabla(\phi\langle\varepsilon\rangle^i)\right] + \frac{\langle\varepsilon\rangle^i}{\langle k\rangle^i}\left[c_1 P^i + c_2 f_2 G^i - c_2 f_2\rho\phi\langle\varepsilon\rangle^i\right] \tag{7}$$

where $P^i = (-\rho\langle\overline{\mathbf{u}'\mathbf{u}'}\rangle^i : \nabla\bar{\mathbf{u}}_D)$ is the production rate of $\langle k\rangle^i$ due the gradients of $\bar{\mathbf{u}}_D$ and $G^i = c_k\rho\frac{\phi\,\langle k\rangle^i|\bar{\mathbf{u}}_D|}{\sqrt{K}}$ is the generation rate of $\langle k\rangle^i$ due to the action of the porous matrix. In Eqs. (5), (6) and (7), c_μ=0.09, σ_k=1.4, σ_ε=1.3, c_1=1.5 and c_2=1.9 are non-dimensional empirical constants proposed by [1] for the $k-\varepsilon$ Low-Reynolds turbulence model. Also, f_2 and f_μ are damping functions of the $k-\varepsilon$ Low-Reynolds model. If f_2=1 and f_μ=1, the turbulent model becomes equal to the $k-\varepsilon$ High-Reynolds model. Specifically for the porous medium, the constant c_k was calculated as being equal to 0.28 through numerical calculations (see [29], [31], [30]).

3.1 Boundary Conditions

Fully developed profiles of velocity, k and ε were employed at the pipe inlet and all derivatives in the axial direction were set to zero at the pipe outlet. Also, non-slip conditions were applied on the walls.

Close to the solid walls the $k-\varepsilon$ Low-Reynolds model uses two damping functions f_2 and f_μ proposed by [1]:

$$f_2=\left\{1-\exp\left[-\frac{(\nu\varepsilon)^{0,25}n}{3,1\nu}\right]\right\}^2\left\{1-0,3\exp\left[-\left(\frac{(k^2/\nu\varepsilon}{6,5}\right)^2\right]\right\} \tag{8}$$

$$f_\mu=\left\{1-\exp\left[-\frac{(\nu\varepsilon)^{0,25}n}{14\nu}\right]\right\}^2\left(1+\frac{5}{(k^2/\nu\varepsilon)^{0,75}}\exp\left\{-\left[\frac{(k^2/\nu\varepsilon)}{200}\right]^2\right\}\right) \tag{9}$$

In Eqs. (8) and (9), n is the normal distance from the wall. In order to use this model, the first volume (whose distance from the wall is denoted n_p) should be placed in the sublayer region. In this innermost region, the viscous effects are dominant comparing with the turbulent effects ($\mu_t << \mu$). Thus, in order to take account the viscous effects of this region, it is advisable that most first volumes has $n_p^+ <1$. $n^+=(u_\tau n/\nu)$ is a non-dimensional distance from the wall, where $u_\tau=(\tau_w/\rho)^{1/2}$ is the friction velocity and ν the kinematic viscosity. Also, τ_w is the shear stress on the wall.

4 Numerical Method

Equations (1), (2), (6) and (7) are discretized for a bi-dimensional axisymmetric domain, in generalized coordinates, involving both clean and porous media. In order to solve the discretized equations system, the control volume approach is employed and, the SIMPLE algorithm is used for handling the velocity-pressure coupling [27]. The Flux Blended Deferred scheme is used for the interpolation functions of the convective flux (more details in [19]). For more details about the numerical method implemented, see [31].

In order to verify grid independence, besides the grid with 34,103 control volumes, two additional grids were generated, one in a coarser mesh with 18,441 control volumes and other in a refined mesh with 65,188 control volumes. The grid nodes were refined toward the wall in order to guarantee the $n_p^+ <1$ condition in most of the first grid points from the wall. The k_c

(contraction minor loss coefficient to be explained in details in the following section) numerical values obtained were 0.601 for the coarser mesh and 0.602 for the refined mesh, with a difference of 1.0%. Therefore, the grid with 34,103 control volumes, used for all numerical calculation in this work, can be considered mesh independent.

Residues of all transport equations involved were calculated at each iteration, having as a convergence criterion a maximum normalized residue equals to 10^{-7}.

5 Results and discussion

5.1 Clear flow

The geometry here considered is a pipe that suffers a sudden contraction with σ=0.1. The geometrical dimensions are here presented as function of the outlet pipe radius, r_{ex}= 0.32 m. In order to consider both the pipe inlet and outlet influence on the flow pattern negligible, the upstream and downstream pipe length were set to be, respectively, $l_{in}/r_{ex} = 9.375$ and $l_{ex}/r_{ex} = 37.5$. Results were obtained considering an outlet Reynolds number of 158,114 based on the outlet pipe diameter (d_{ex}), as shown:

$$Re_{ex} = \frac{U_{ex} d_{ex}}{\nu} \tag{10}$$

where U_{ex} is the outlet pipe streamwise bulk velocity.

The numerical simulation (using $k - \varepsilon$ Low-Reynolds model) was also performed in a pipe without changes in its diameter, that is, all the pipe was kept with the pipe inlet diameter, d_{in}. The Reynolds number used in the numerical calculations, which is based on the pipe inlet diameter, is given by:

$$Re_{in} = \frac{U_{in} d_{in}}{\nu} = 50,000 \tag{11}$$

In order to validate the code, the velocity profile obtained from the numerical calculations for the straight pipe was compared with the correspondent experimental results of Laufer (1954), [22], and also with the wall logarithmic law. In the calculations, a spatial periodicity condition between the inlet and the outlet pipe was employed. The grid points were refined on the wall in order to have $n_p^+ < 1$. Figure 3 shows that the present results have a good agreement with the experimental results of [22] and follow the wall logarithmic law ($n^+ > 11.225$, κ=0.42 and E=9.0) and the laminar sublayer ($0 < n^+ < 11.225$).

Simulation considering the sudden pipe contraction without the porous insert was carried out and the minor loss obtained from that calculations was compared with an experimental result available in the literature, Streeter (1961), [34]. Imposed fully developed inlet profiles of velocity, k and ε were obtained from the experimental results of [22].

The minor loss (h_c) can be defined as:

$$h_c = k_c \frac{U_{ex}^2}{2g} \tag{12}$$

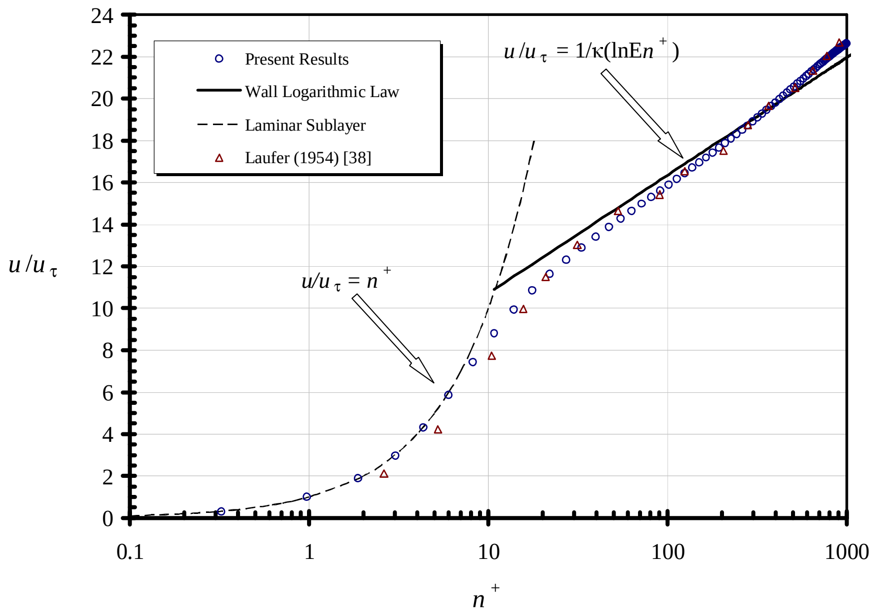

Figure 3: Comparison of velocity profile in the unchanging section pipe-flow for $Re_{in} = 50,000$.

where, k_c is the contraction minor loss coefficient (non-dimensional value). This value does not account for the major losses but only for the minor losses due to the contraction.

In [34], the experimental values of k_c are presented for several geometries for turbulent flows. Due to the fact that k_c is not significantly affected with the Reynolds number in fully turbulent flows, the experimental values of [34] are presented independently of the Reynolds number. Thus, according to [34], for $Re_{ex} = 158,114$ and $\sigma = 0.1$, one has $k_c = 0.46$ (see [34], pp. 3-21, Tab. 3.2).

Figure 4 shows the pressure coefficient, Cp which is obtained through numerical calculations and can be defined as:

$$Cp = \frac{p - p_{ref}}{0.5\rho U_{ex}^2} \tag{13}$$

where p_{ref} is a reference pressure adopted as zero and p is a pressure of any point in the flow domain. Thus, according to k_c and Cp definitions and with some algebraic manipulation, the value of k_c is given by:

$$k_c = (Cp_{in} - Cp_{ex}) + (U_{in}^2/U_{ex}^2) - 1 \tag{14}$$

where subscripts in and ex refer to the inlet and outlet pipe, respectively. As shown in Fig. 4, Cp_{in} and Cp_{ex} can be determined from the Cp values upstream and downstream the duct contraction by extrapolating their linear pressure courses to the transitional cross section.

According to the numerical calculations, the k_c value obtained is 0.596, which is 30% higher than the experimental result of k_c (see [34], pp. 3-21, Tab. 3.2). The difference between

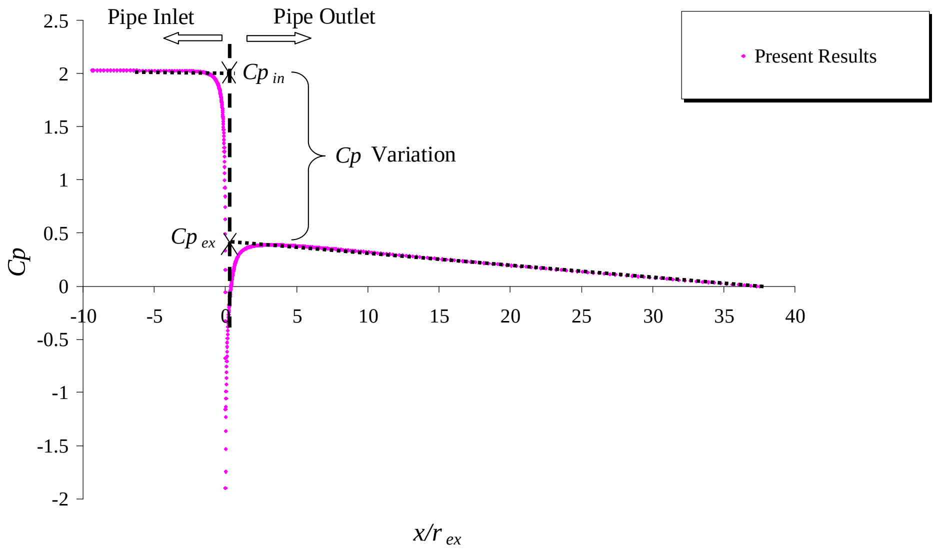

Figure 4: Numerical results of Cp along the pipe walls for Re_{ex}= 158,114, without porous insert.

experimental and numerical results is probably due to limitations of the turbulence model used and to the lack of information about the experimental procedure employed.

6 Porous Insert

In this section, results for a pipe with a sudden contraction and with a porous insert are presented. Four values of permeability, K, and two different thicknesses (a) are used in the numerical simulations. The Reynolds number is 158,114 and the porosity, ϕ, is 0.99. In all figures below, results are shown along the axial coordinate and the radial position is fixed on the wall.

The *vena contracta* is the main responsible for the minor losses due to the contraction. Therefore, one of the objectives of the porous insert is to reduce or suppress the recirculating bubble, although the porous insert itself increases the losses. So, there is a compromise between the losses caused by the porous insert and the gain in eliminating or diminishing the recirculating bubble. Thus, as a first approach, a porosity of 0.99 is here adopted in order to minimize the minor losses caused by the porous insert. An example of such porous insertion with high porosity could be represented as a set of parallel thin blades. Additionally, four different permeabilities are considered in order to analyze the influence of the porous insert permeability on the flow behavior.

Figures 6 and 7 show the influence of the porous insert permeability on the Cp values along the pipe length. According to Figs. 6 and 7, it is noted that the lower the permeability, the higher the variation of Cp values through the porous insert. Also, it is observed that the minimum

Cp values increase when the permeability is decreased which can possibly minimize occasional cavitation problems.

It is import to emphasize that, the region used to show the results in Figs. 8-11 is represented by the area surrounded by dashed lines located at the pipe contraction region showed in Fig. 5.

Figures 8 and 9 present the recirculating bubble streamlines attached to the wall past the contraction. It is observed that, as the value of the porous insert decreases, the recirculation length is reduced, which indicates a damping effect on the recirculating bubble due to the porous insert. Also, it is noticed that the recirculation length is not significantly affected when the two different thicknesses ($a = 0.312$ and $a = 0.625$) with same permeability are considered.

Figures 10 and 11 show the normalized kinetic turbulent energy field (KN). According to Figs. 10 and 11, it is observed that, as the permeability decreases, the higher KN values are found to be more confined inside the porous insert, mainly in the vicinity of the contraction corner, due to the higher generation of turbulent kinetic energy in such region.

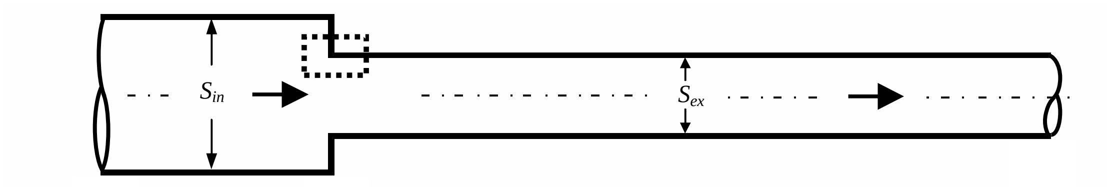

Figure 5: Sketch of the pipe with a sudden contraction showing an area surrounded by dashed lines.

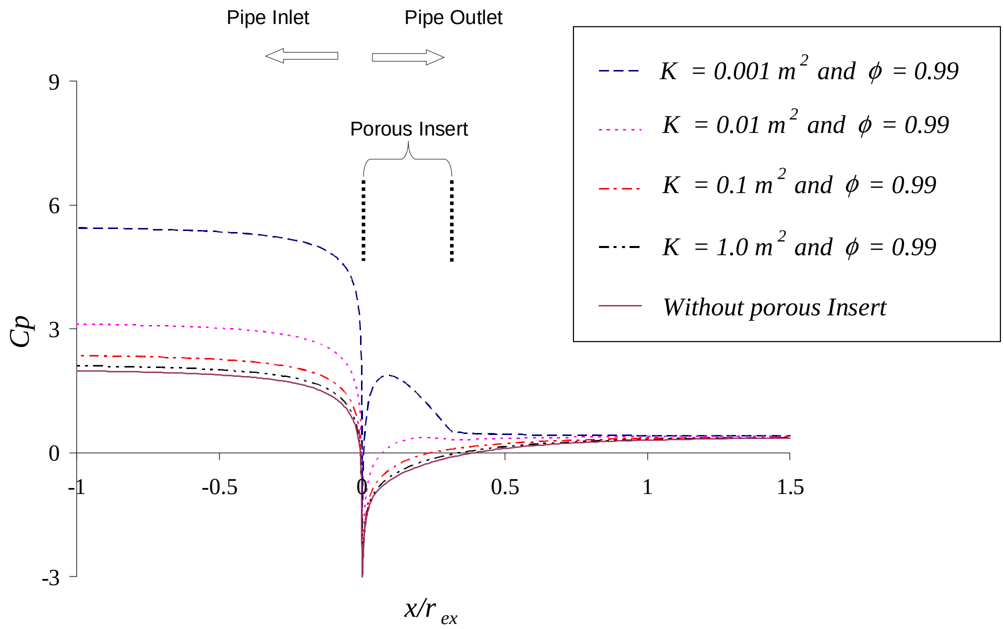

Figure 6: Cp values along the pipe walls, with and without the porous insert, $Re_{ex} = 158,114$ and $a/r_{ex} = 0.312$.

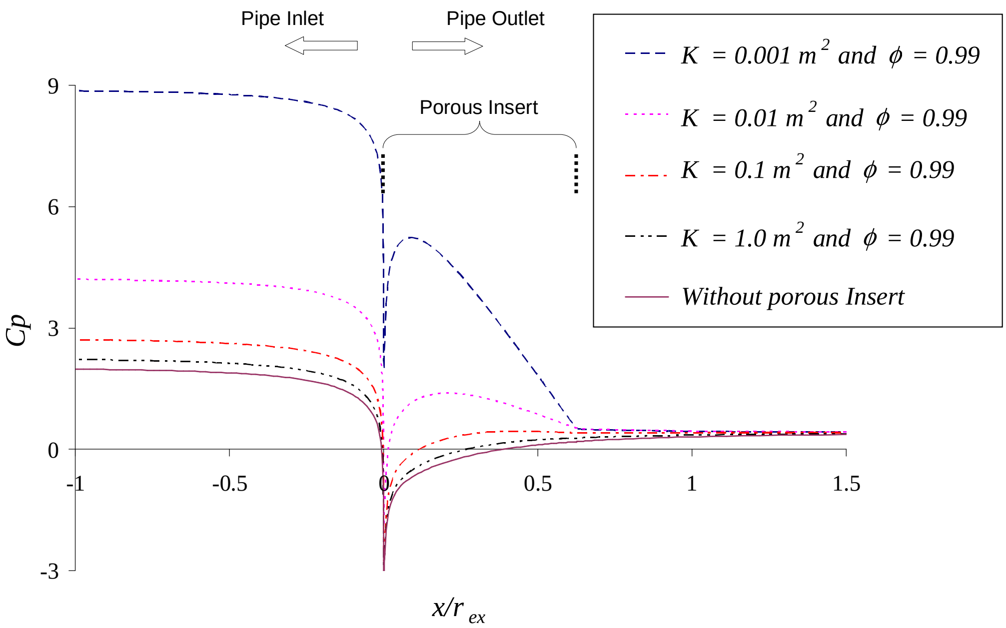

Figure 7: Cp values along the pipe walls, with and without the porous insert, $Re_{ex} = 158,114$ and $a/r_{ex} = 0.625$.

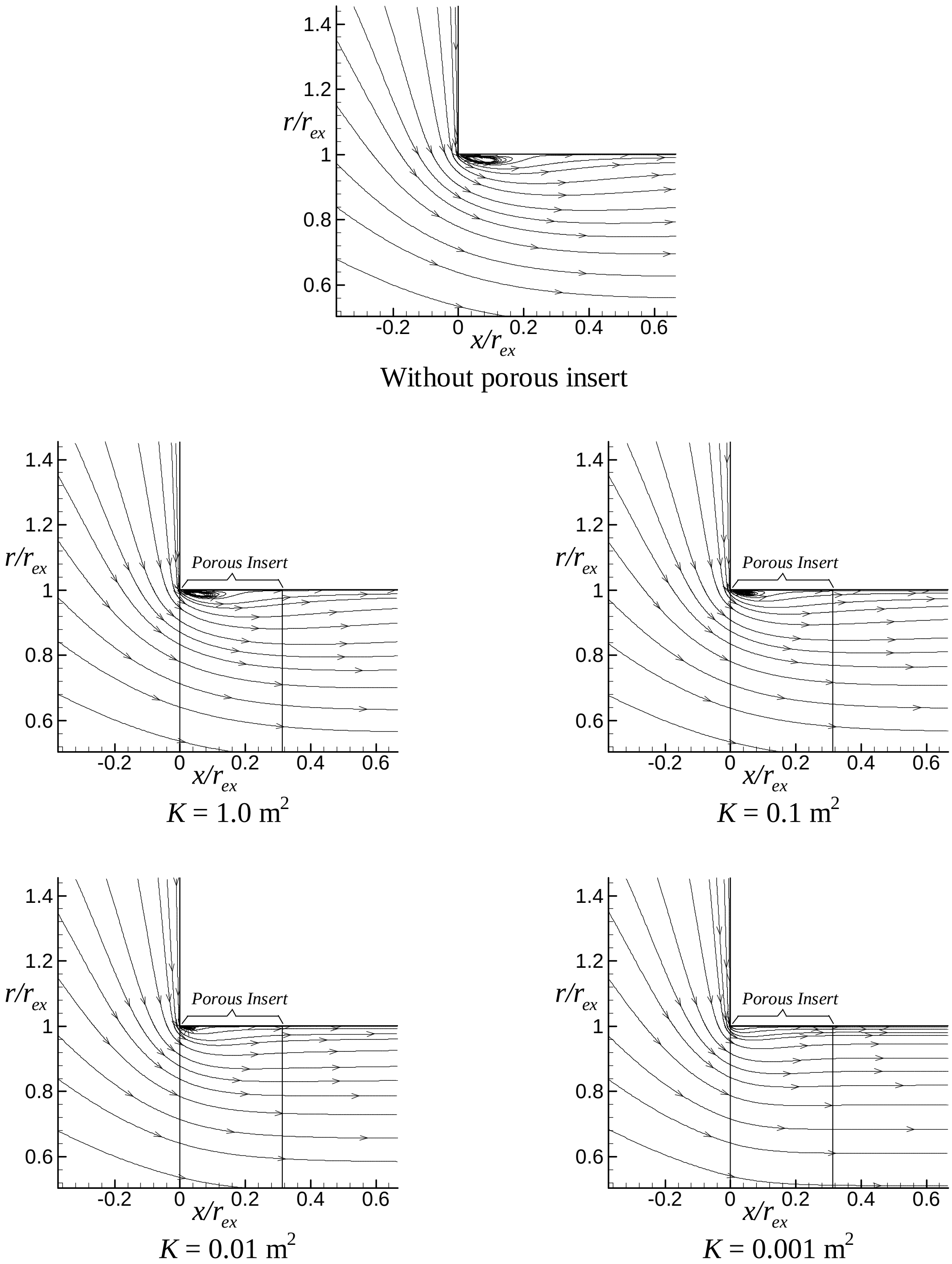

Figure 8: Streamlines at the region surrounded by dashed lines showed in Fig. 5 − $Re_e x =$ 158,114 - $a/r_{ex} = 0.312$.

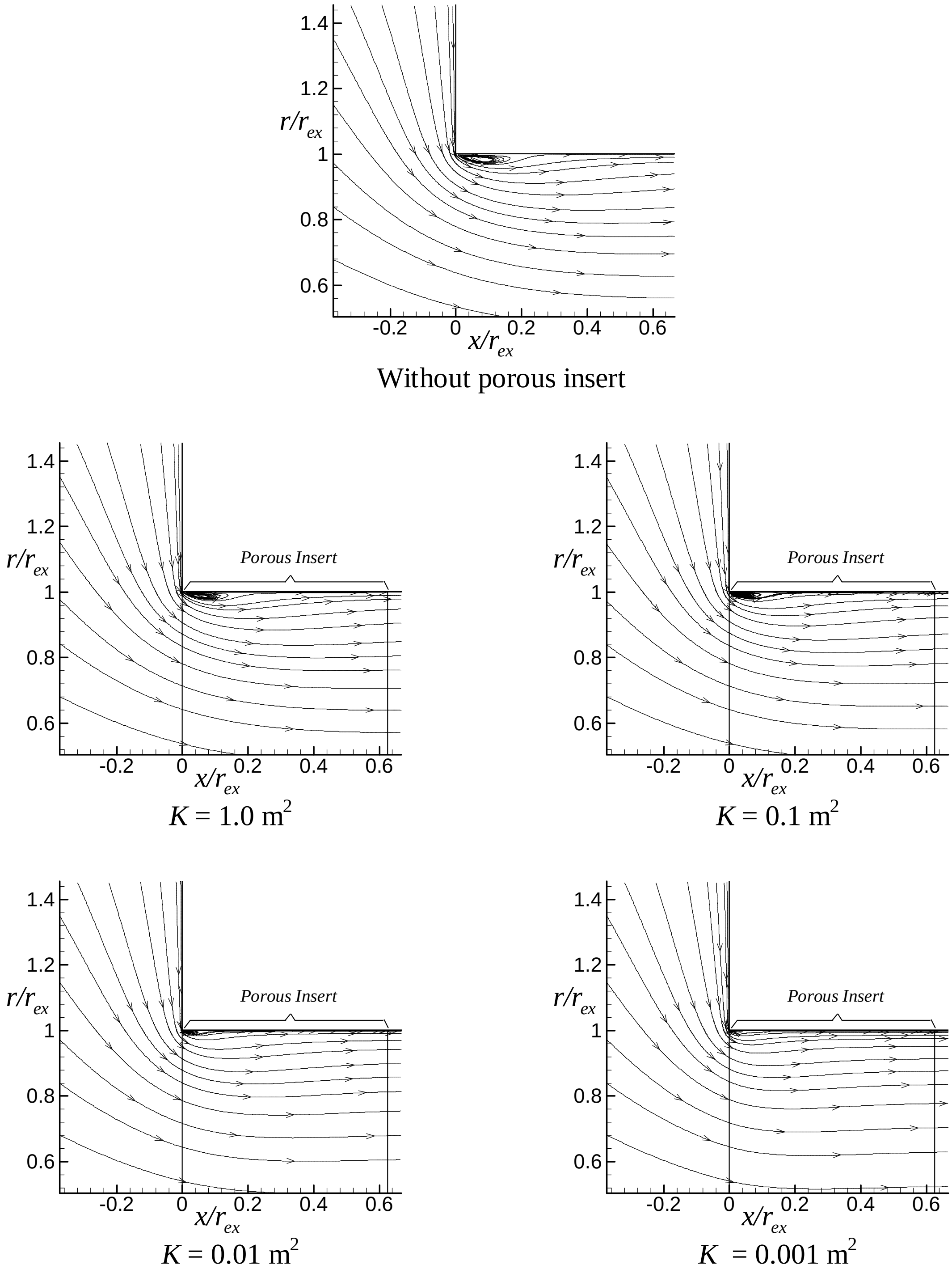

Figure 9: Streamlines at the region surrounded by dashed lines showed in Fig. 5 – Re_{ex} = 158,114 - $a/r_{ex} = 0.625$.

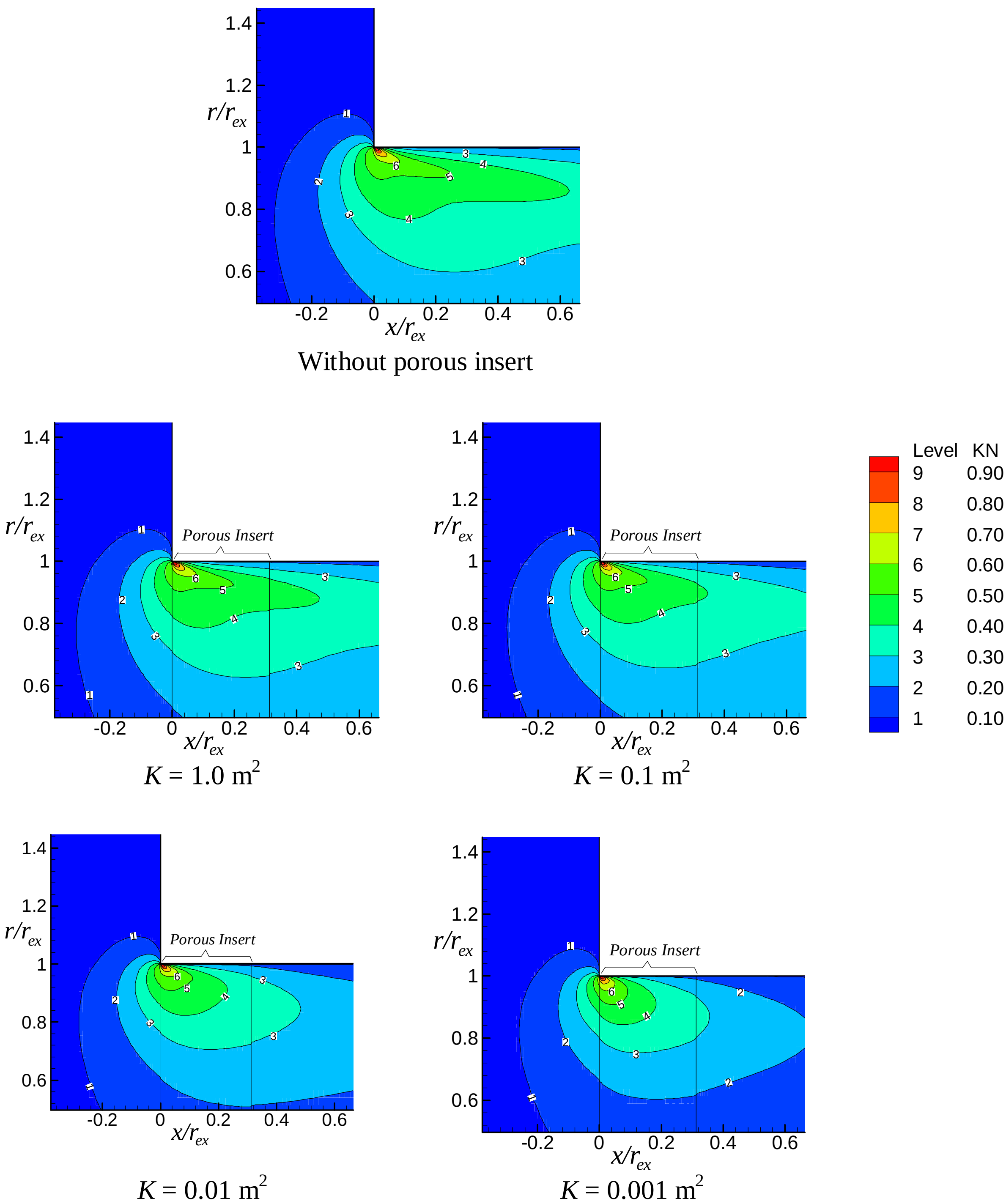

Figure 10: Normalized turbulent kinetic energy (KN) field at the region surrounded by dashed lines showed in Fig. 5, Re_{ex} = 158,114 and $a/r_{ex} = 0.312$.

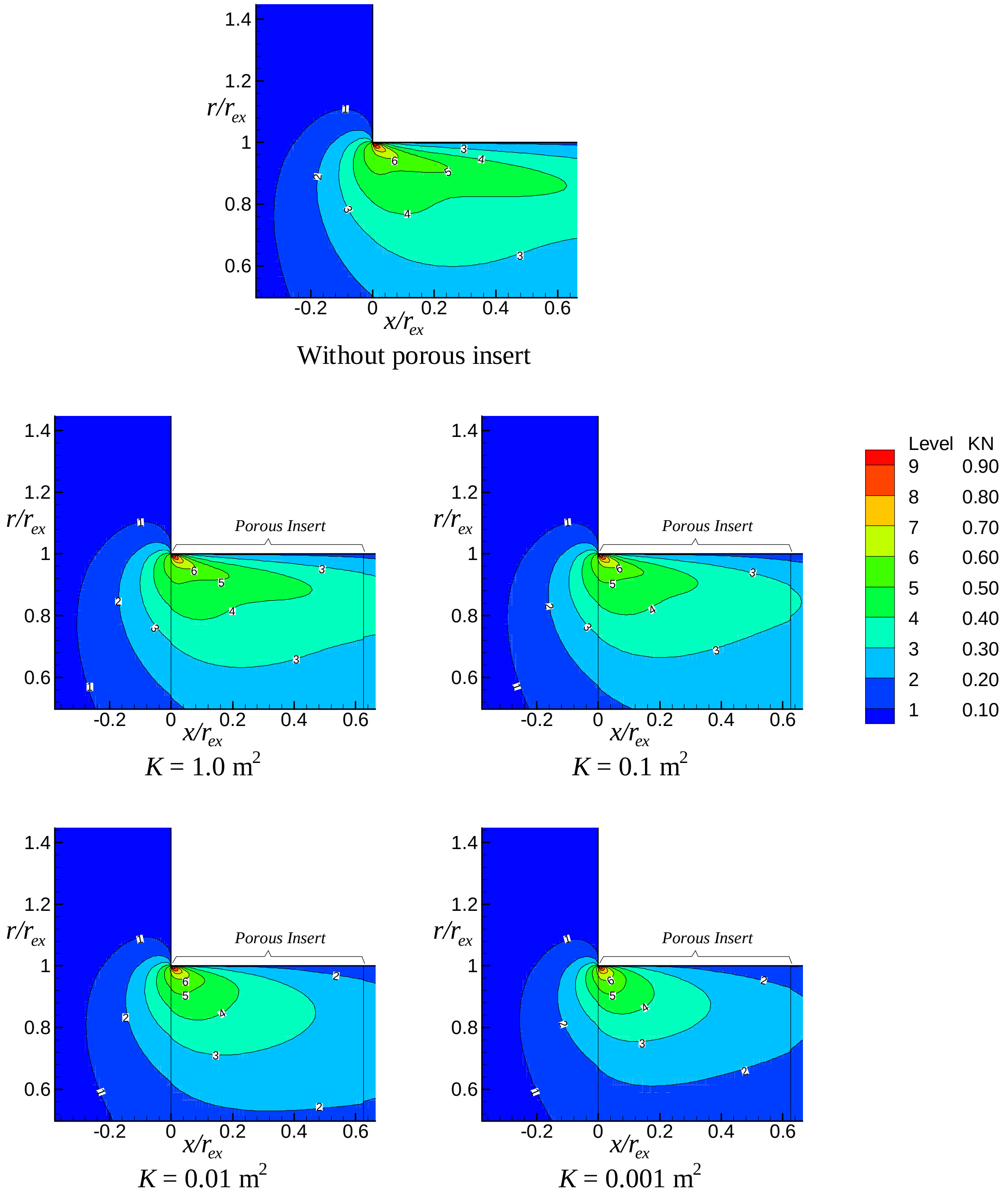

Figure 11: Normalized turbulent kinetic energy (KN) field at the region surrounded by dashed lines showed in Fig. 5, $Re_{ex} = 158{,}114$ and $a/r_{ex} = 0.625$.

Figure 12 and 13 show the C_f (friction coefficient) values along the pipe outlet wall, where C_f is defined as follows:

$$C_f = \frac{\tau_w}{\rho U_{ex}^2/2} \tag{15}$$

In Figs. 12 and 13, the negative C_f values indicate the existence of a recirculation. Thus, it is possible to evaluate the recirculation length by taking the distance from the contraction corner to the point where the C_f value becomes positive. Then, according to Figs. 12 and 13, it is noticed that the recirculation length is not significantly affected when the two different thicknesses ($a/r_{ex} = 0.312$ and $a/r_{ex} = 0.625$) are compared considering the same permeability, which is in accordance with the remarks of Figs. 8 and 9.

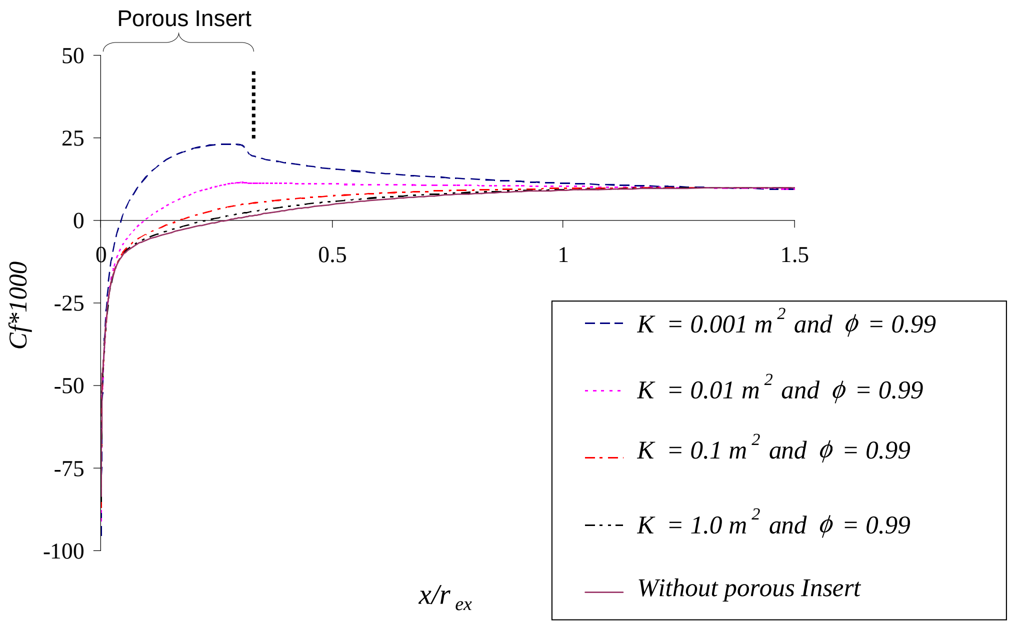

Figure 12: C_f values along the pipe outlet wall - $Re_{ex} = 158{,}114 - a/r_{ex} = 0.312$

Considering the Cp values plotted as function of the pipe length from its inlet until its outlet for each porous insert and, then, extrapolating its courses upstream and downstream the contraction to the transitional cross section (as shown in Fig. 4), the k_c value for each case can be obtained. Thus, Tables 1 and 2 present the obtained k_c values as function of K for $a/r_{ex} = 0.312$ and $a/r_{ex} = 0.625$, respectively.

In addition, in order to show the behavior of the k_c values as function of the permeability, the present results of Table 1 and 2 are also shown in Fig. 14.

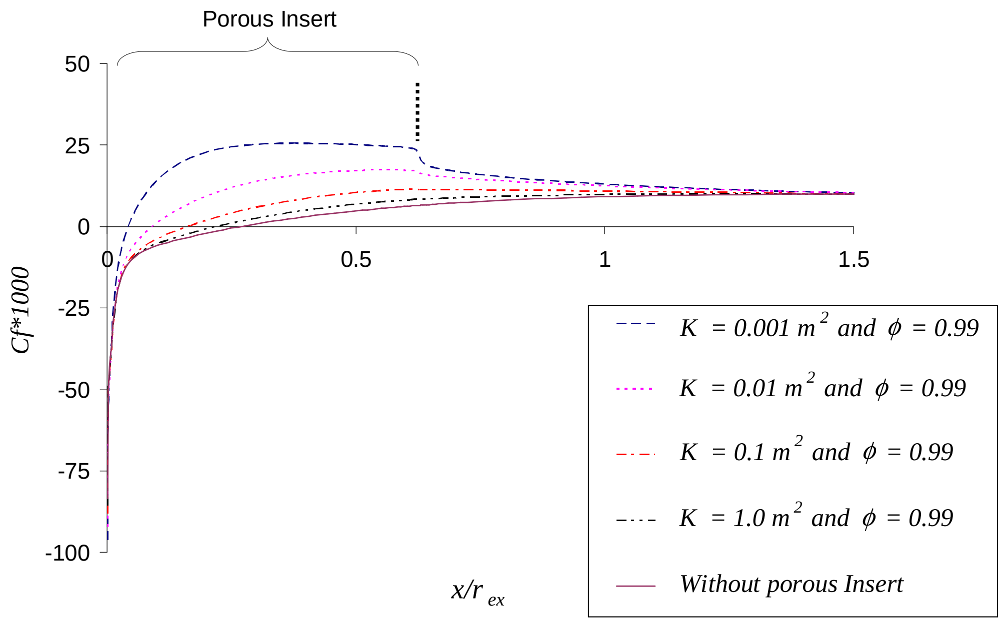

Figure 13: C_f values along the outlet pipe wall, Re_{ex} = 158,114 and a/r_{ex} = 0.625.

Table 1: k_c values as function of K for $a/r_{ex} = 0.312$

	$a/r_{ex} = 0.312$			
K [m^2]	0.001	0.01	0.1	1.0
k_c	4.09	1.74	0.98	0.72

Table 2: k_c values as function of K for $a/r_{ex} = 0.625$

	$a/r_{ex} = 0.625$			
K [m^2]	0.001	0.01	0.1	1.0
k_c	7.52	2.84	1.33	0.84

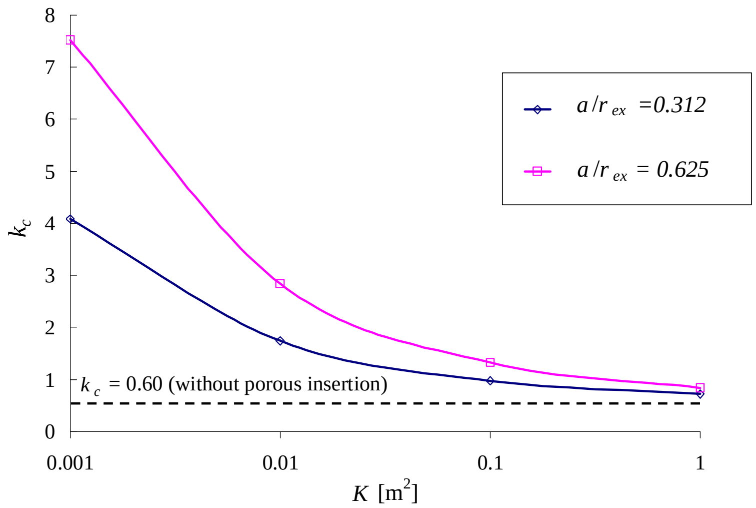

Figure 14: Behavior of k_c (pipe minor loss coefficient) with K (permeability) for $a/r_{ex} = 0.312$ and $a/r_{ex} = 0.625$.

7 Concluding remarks

This work study the porous insert influence on a turbulent flow in a pipe which suffers a sudden contraction. The numerical tool employed is the control volume technique in a generalized co-ordinate system. The turbulent model used is the macroscopic $k - \varepsilon$ Low-Reynolds turbulence model. First, the numerical result of the flow in the pipe without porous insert was compared with an experimental result available in the literature. Afterwards, the same pipe was investigated with a porous insert placed past the contraction.

According to the numerical calculations, the k_c value obtained for a sudden contraction without a porous insert was 30% higher than the experimental result of [34]. The difference between experimental and numerical results is probably due to limitations of the turbulence model used and to the lack of information about the experimental procedure employed.

It was noticed that all porous inserts considered reduce the recirculation size past the contraction when compared with the case without the porous insert. Also, the recirculation length is not significantly affected when the two different thicknesses with same permeability, K, are considered. Although the recirculation size is reduced due to the porous insert, the minor losses are always higher than the case without porous insert. Therefore, according to the numerical results, one can conclude that the losses caused by the porous insert itself are more significant than the gain due to the reduction of the recirculating bubble. Despite of the increase of the pressure losses due to the porous insert in the pipe, the attenuation or even the suppression of the recirculating bubble could be useful in some industrial process, in order to regulate the flux downstream the pipe contraction.

For future works, the authors intend to analyze the pipe by employing a non-linear turbulence model since, in [10], better results were obtained with the use of such model.

Acknowledgements: The authors are thankful to CNPq and FAPESP, Brazil, for their financial support during the course of this research.

References

[1] K. Abe, Y. Nagano, and T. Kondoh. An improved k-ε model for prediction of turbulent flows with separation and reattachment. *Trans. JSME, Ser. B.*, 58:3003–3010, 1992.

[2] B.V. Antohe and J.L. Lage. A general two-equation macroscopic turbulence model for incompressible flow in porous media. *Int. J. Heat Mass Transfer*, 40:3013–3024, 1997.

[3] M. Assato and M.J.S. de Lemos. Turbulent heat transfer in an abrupt contraction channel with a porous obstacle using a non-linear model with a high reynolds number wall function. In *III Cong. National de Eng. Mecânica*, Belém, Brazil, 10-13 August, 2004.

[4] M. Assato and M.J.S. de Lemos. Tratamento numérico e aplicações de um modelo de viscosidade turbulenta não linear para alto e baixo reynolds (in portuguese). In *Escola Brasileira de Primavera Transição e Turbulência*, pages 11–15, Uberlândia, Brazil, 11-14 Dec, 2000.

[5] M. Assato and M.J.S. de Lemos. Simulation of heat transfer in a forward-facing step flow with a porous insert using linear and non-linear k-ε models. In *Int. Conf. on Porous Media and Applications*, Évora, Portugal, 24-27 May, 2004.

[6] M. Assato and M.J.S. de Lemos. Heat transfer in a back-step flow past a porous insert using a non-linear turbulence model and a low reynolds wall treatment. In *3rd Int. Conf. on Computational Heat and Mass Transfer*, Banff, Canada, 26-30 May, 2003. Univ. of Calgary.

[7] M. Assato and M.J.S. de Lemos. Estudo da transferência de calor turbulenta em uma contração abrupta com inserto poroso usando modelos de turbulência linear e não linear (in portuguese). In *Proc. 10th Brazilian Cong. Thermal Sciences and Eng.*, Rio de Janeiro, Brazil, Nov. 29-Dec. 03, 2004b. on CD-ROM.

[8] M. Assato and M.J.S. de Lemos. Heat transfer in a suddenly expanded turbulent flow past a porous insert using linear and non-linear eddy-viscosity models. *ASME Int. Mechanical Eng. Congress and Exposition*, November, 2002.

[9] M. Assato and M.J.S. de Lemos. Flow and heat transfer past a sudden contraction with a porous insert using linear and non-linear turbulence models. In *Proc. IMECE2004, ASME Int. Mechanical Eng. Congress*, Anaheim, CA, USA, November, 2004d.

[10] M. Assato, M.H.J. Pedras, and M.J.S. de Lemos. Numerical solution of turbulent flow past a backward-facing-step with a porous insert using linear and non-linear k-ε models. *J.Porous Media*, 8(1):13–29, 2005.

[11] G. Astarita and G. Greco. Excess pressure drop in laminar flow through sudden contraction. *I & EC Fundamentals*, 7(1):27–31, 1968.

[12] C.C. Chan and F-S Lien. Permeability effects of turbulent flow through a porous insert in a backward-facing-step channel. *Transport in Porous Media*, 59(1):47–71, 2005.

[13] M.J.S. de Lemos and M.H.J. Pedras. Recent mathematical models for turbulent flow in saturated rigid porous media. *J. Fluids Eng.*, 123:935–940, 2001.

[14] M.J.S. de Lemos and L.A. Tofaneli. Pressure drop characteristics of parallel-plate channel flow with porous obstructions at both walls. In *Proc. IMECE2003, ASME Int. Mechanical Eng. Congress*, Washington, D.C., USA, Novemeber, 2003.

[15] F. Durst and T. Loy. Investigations of laminar flow in a pipe with sudden contraction of cross sectional area. *Comp. & Fluids*, 13(1):15–36, 1985.

[16] D. Getachewa, D.W.J. Minkowycz, and J.L. Lage. A modified form of the k–ε model for turbulent flow of an incompressible fluid in porous media. *Int. J. Heat Mass Transfer*, 43:2909–2915, 2000.

[17] W.G. Gray and P.C.Y. Lee. On the theorems for local volume averaging of multiphase system. *Int. J. Multiphase Flow*, 12:401–410, 1977.

[18] I.E. Idelcick. *Memento des pertes de charges.* Editeur Paris, 1960.

[19] P.K. Khosla and S.G. Rubin. A diagonally dominant second-order accurate implicit scheme. *Comp. & Fluids*, 2:207, 1974.

[20] F. Kuwahara, Y. Kameyama, S. Yamashita, and A. Nakayama. Numerical modeling of turbulent flow in porous media using a spatially periodic array. *J. Porous Media*, 1:47–55, 1998.

[21] K. Kuwahara and A. Nakayama. Numerical modeling of non-darcy convective flow in a porous medium. In *Proc. 11th Int. Heat Transfer Conf.*, Kyongyu, Korea, August 23–28, 1998.

[22] J. Laufer. The structure of turbulence in fully developed pipe flow. *NACA Tech. Repts.*, 1174, 1954.

[23] K. Lee and J.R. Howell. Forced convective and radiative transfer within a highly porous layer exposed to a turbulent external flow field. In *Proc. ASME-JSME Thermal Eng. Joint Conf.*, volume 2, pages 377–386, 1987.

[24] T. Masuoka and Y. Takatsu. Turbulence model for flow through porous media. *Int. J. Heat Mass Transfer*, 39:2803–2809, 1996.

[25] A. Nakayama and F. Kuwahara. A macroscopic turbulence model for flow in a porous medium. *ASME J. Fluids Eng.*, 121:427–433, 1999.

[26] R.M. Orselli and M.J.S. de Lemos. Escoamento turbulento em contração súbita com inserto poroso (in portuguese). In *Proc. 10th Braz. Cong. Thermal Sciences Eng.*, Rio de Janeiro, Brazil, Nov. 29-Dec. 03, 2004. on CD-ROM.

[27] S.V. Patankar. *Numerical heat transfer and fluid flow.* Mc-Graw Hill, 1980.

[28] M.H.J. Pedras and M.J.S. de Lemos. On the definition of turbulent kinetic energy for flow in porous media. *Int. Commun. Heat and Mass Transfer*, 27(2):211–220, 2000.

[29] M.H.J. Pedras and M.J.S. de Lemos. Macroscopic turbulence modeling for incompressible flow through undeformable porous media. *Int. J. Heat Mass Transfer*, 44(6):1081–1093, 2001.

[30] M.H.J. Pedras and M.J.S. de Lemos. On the mathematical description and simulation of turbulent flow in a porous media formed by an array of elleptic rods. *J. Fluids Eng.*, 123(4):941–947, 2001.

[31] M.H.J. Pedras and M.J.S. de Lemos. Simulation of turbulent flow in porous media using a spatially periodic array and a low re two-equation closure. *Numerical Heat Transfer - Part A Applications*, 39(1):35–59, 2001.

[32] F. D. Rocamora Jr. and M.J.S. de Lemos. Numerical solution of turbulent flow in porous media using a spatially periodic array and the k-ε model. In *Proc. ENCIT-98—7th Braz. Cong. Thermal Sciences Eng.*, volume 2, pages 1265–1271, Rio de Janeiro, Brazil, 1998.

[33] F. D. Rocamora Jr. and M.S.J. de Lemos. Analysis of convective heat transfer for turbulent flow in saturated porous media. *Int. Commun. Heat Mass Transfer*, 27(6):825–834, 2000.

[34] V.L. Streeter. *ed. Handbook of Fluid Dynamics.* McGraw-Hill, New York, 1961.

[35] Y. Takatsu and T. Masuoka. Turbulent phenomena in flow through porous media. *J. Porous Media*, 1(3):243–251, 1998.

[36] J.S. Vrentas and J.L. Duda. Flow of a newtonian fluid through a sudden contraction. *Applied Scientific Research*, 28:241–261, 1973.

[37] H. Wang and E.S. Takle. Boundary-layer flow and turbulence near porous obstacles. *Boundary Layer Meteorol.*, 74:73–88, 1995.

[38] J. Weisbach. *Die experimeantal-hydraulick.* J.S. Englehardt, Freiburg, 1855.